

A Probabilistic Distance-Based Stability Quantifier for Complex Dynamical Systems

C. Alvares¹ and S. Banerjee²

¹*Department of Physical Sciences, Indian Institute of Science Education and Research Kolkata, Mohanpur, 741 246, India*

²*Department of Physical Sciences, Indian Institute of Science Education and Research Kolkata, Mohanpur, 741 246, India*

(*Electronic mail: soumitro@iiserkol.ac.in.)

(*Electronic mail: alvarescalvin16@gmail.com)

(Dated: 3 November 2023)

For a dynamical system, an attractor of the system may represent the ‘desirable’ state. Perturbations acting on the system may push the system out of the basin of attraction of the desirable attractor. Hence, it is important to study the stability of such systems against reasonably large perturbations. We introduce a distance-based measure of stability, called ‘stability bound’, to characterize the stability of dynamical systems against finite perturbations. This stability measure depends on the size and shape of the basin of attraction of the desirable attractor. A probabilistic sampling-based approach is used to estimate stability bound and quantify the associated estimation error. An important feature of stability bound is that it is numerically computable for any basin of attraction, including fractal basins. We demonstrate the merit of this stability measure using an ecological model of the Amazon rainforest, a ship capsizing model, and a power grid model.

Many systems, such as the human brain, ecosystems, and power grids, have one or more stable attracting states. In such systems, it might be desirable for the system to function in a specific attracting state. However, perturbations acting on a system can cause the system to move out of this desirable state and into an undesirable state. Thus, it is necessary to study how stable such systems are against perturbations acting on them. For a specific attractor, the set of points in the phase space that converge to the attractor is called its basin of attraction. Perturbations that push the system into states that are not part of the basin of attraction of the desirable attractor are unsafe for the system. Thus, the volume and structure of the basin of attraction of the desirable attractor can aid in quantifying the stability of a system. We propose a measure called *stability bound*, which quantifies the stability of dynamical systems against finite perturbations. Using three example systems — an ecological model of the Amazon rainforest, a ship capsizing model, and a power grid model, we show that the proposed measure gives a reliable indication of the possibility of failure of a system when the system is perturbed away from the desirable attractor.

Linear stability analysis, which involves the evaluation of the eigenvalues of the Jacobian matrix at an equilibrium point or the master stability function⁶, quantifies the local stability of a system. However, since perturbations affecting systems can be large, linear stability analysis cannot be employed to quantify the stability of a system against finite perturbations. To deal with the effect of finite perturbations, the analytic method of Lyapunov functions⁷ is often used to estimate basins of attractions and thus act as a quantifier of stability. However, Lyapunov functions are extremely hard to construct for many dynamical systems.

There exist several non-analytical approaches to quantify the stability of a system against finite perturbation^{8–14}. These stability quantifiers are related to the basin of attraction of the desirable attractor. A popular measure of stability against finite perturbations known as basin stability^{8,15} relates to the volume of the attractor’s basin of attraction. The basin stability of an attractor is defined as the fraction of states that are part of the attractor’s basin of attraction in a finite subset of the phase space. To numerically estimate basin stability, a Monte Carlo simulation is used. This involves sampling points in a finite region of the phase space, and counting the number of points that are part of the attractor’s basin of attraction. The ratio of the number of points in the basin of attraction to the total number of points sampled estimates basin stability. A key feature of basin stability is that computation is numerically tractable for high-dimensional systems, as the standard error associated with the estimation only depends on the number of points sampled and not on the dimension of the system. Basin stability, however, is dependent on *a priori* phase space region in which it is defined. Moreover, basin stability does not say anything about the minimum perturbation that can push the system out of its basin of attraction.

The stability of a system can also be characterized by the shortest distance from the attractor to the boundary of the

I. INTRODUCTION

Dynamical system models of real-world phenomena often contain more than one attractor¹, one of which can be an ‘attractor at infinity’. Some examples of such systems include the human brain², ecosystems³, climate systems⁴, and power grids⁵. In such systems, it is generally desirable for the system to be in a specific attractor. Studying the response of the system in the desirable attractor to perturbations can aid in quantifying the system’s stability.

basin of attraction^{12,16,17}. This shortest distance stability measure has recently been labeled stability threshold¹². It is equal to the minimum perturbation that can push the system out of the basin of attraction. However, the stability threshold is numerically computable only for smooth basin boundaries. Systems can often have fractal basins¹⁸. The stability threshold is not computable for such systems.

To deal with the drawbacks of basin stability and stability threshold, we propose a distance-based stability quantifier, called stability bound, that is computable for all types of basin of attraction. Like basin stability, a probabilistic sampling-based procedure is used to compute the stability bound. Since the phase space of a dynamical system can be unbounded, stability bound is computed over a finite subset of the phase space. However, unlike basin stability, the value of the stability bound does not directly depend on the chosen phase space region. If the chosen phase space region is large enough, the stability bound is independent of it.

This paper is organized as follows. We define the stability bound in section II and outline the method of its computation. In section III, we demonstrate the applicability of this stability measure to various dynamical systems. Section IV concludes the work.

II. STABILITY BOUND

A. Definition

Consider an N dimensional dynamical system with phase space X and at least one finite attractor. The basin stability of an attractor \mathcal{A} of the dynamical system is defined as^{8,15}

$$S_B(X_P) = \int \chi(x) \rho(x, X_P) dx \quad (1)$$

where $x \in X$, and X_P is a bounded subset of the phase space representing the states to which the system can be perturbed. $\chi(x)$ indicates whether a state is in the basin of attraction \mathcal{B} of the attractor \mathcal{A} . $\chi(x)$ is defined as

$$\chi(x) = \begin{cases} 1 & \text{if } x \in \mathcal{B} \\ 0 & \text{otherwise} \end{cases} \quad (2)$$

$\rho(x, X_P)$ is the probability density of perturbations. It takes non-zero values for $x \in X_P$, such that $\int \rho(x, X_P) dx = 1$.

The probability density function $\rho(x, X_P)$ used to define basin stability is typically taken to be a uniform distribution in the region X_P ^{8,15}. This implies that every perturbation in the region X_P is equally likely. If the state of the system is represented in Cartesian coordinates, then this density function can be written as

$$\rho(x, X_P) = \begin{cases} 1/|X_P| & \text{if } x \in X_P \\ 0 & \text{otherwise} \end{cases} \quad (3)$$

With such a distribution of perturbations, basin stability is defined as

$$S_B(X_P) = \frac{\text{Vol}(X_P \cap \mathcal{B})}{\text{Vol}(X_P)} \quad (4)$$

Throughout this paper, we define basin stability using a uniform distribution of perturbations.

Consider a bounded region $X_0 \subseteq X$ of the phase space. The stability bound is defined in this region. $X_D(d)$ is the set of points within a distance d from the attractor that lie in the set X_0 . It is defined as

$$X_D(d) = \{x \in X_0 \mid \text{dist}(x, \mathcal{A}) < d\} \quad (5)$$

where $\text{dist}(x, \mathcal{A})$ is the distance of the state x to the attractor \mathcal{A} . If \bar{d} is a distance metric on X , then

$$\text{dist}(x, \mathcal{A}) = \inf\{\bar{d}(x, y) \mid y \in \mathcal{A}\} \quad (6)$$

For all the examples in this paper, we use the Euclidean distance as the distance metric, such that

$$\bar{d}(x, y) = \sqrt{\sum_{i=1}^N a_i^2 (x_i - y_i)^2} \quad (7)$$

is the distance between the states $x = (x_1, x_2, \dots, x_N)$ and $y = (y_1, y_2, \dots, y_N)$. We chose a_i to be unity with the dimension of $1/x_i$.

Define a set D , the set of distances at which the corresponding basin stability is less than a basin stability tolerance t . D is written as

$$D = \{d \in (0, d_{\max}] \mid S_B(X_D(d)) < t\} \quad (8)$$

where $t \in (0, 1]$ is the predefined basin stability tolerance, and

$$d_{\max} = \sup\{\text{dist}(x, \mathcal{A}) \mid x \in X_0\}. \quad (9)$$

We define the stability bound as the minimum distance at which the corresponding basin stability is less than the tolerance t . Thus, the stability bound of the attractor \mathcal{A} is

$$B_S = \begin{cases} \inf(D) & \text{if } D \neq \emptyset \\ d_{\max} & \text{otherwise} \end{cases} \quad (10)$$

Here, the distance has been defined in a similar manner as in¹⁹, where it was used to characterize the linear size of basins of attractions. However, this approach is now extended to function as a stability quantifier for dynamical systems.

Although the stability bound is defined in a finite subset X_0 of the phase space, its value would not necessarily depend on this choice. The stability bound depends on the region X_0 if the region $X_D(d)$, corresponding to the stability bound distance $d = B_S$, depends on the choice of X_0 . Thus, if $\exists x \in X$, such that $\text{dist}(x, \mathcal{A}) < B_S \wedge x \notin X_0$, the stability bound B_S depends on the region X_0 . Hence, if X_0 is large enough, the stability bound becomes independent of the choice of X_0 .

B. Numerical computation

A Monte Carlo numerical experiment is used to estimate the basin stability $S_B(X_P)$ ⁸. In the region X_P , a number of initial conditions, n , are sampled from the distribution $\rho(x, X_P)$. If

the number of initial conditions that converge to the attractor \mathcal{A} is n_A , then the estimated basin stability of the attractor is

$$\hat{S}_B(X_P) = \frac{n_A}{n} \quad (11)$$

The basin stability $S_B(X_P)$ is estimated using a Bernoulli-like experiment with n trials. If the probability that a point chosen in the region X_P is in the basin of attraction is p , then the standard error in the estimate of basin stability is

$$e = \sqrt{\frac{p(1-p)}{n}} \quad (12)$$

Thus, $e \leq 0.5/\sqrt{n}$. The estimated basin stability within ± 1 standard deviation is reported as $[\hat{S}_B(X_P) - e, \hat{S}_B(X_P) + e]$.

To compute the stability bound, the basin stability $\hat{S}_B(X_D(d))$ is computed from $d = d_{\max}$ to $d = d_0$, using n samples for every basin stability estimation. d_{\max} is defined in equation (9), and d_0 is the largest distance such that $\hat{S}_B(X_D(d_0)) = 1$. For $\hat{S}_B(X_D(d)) < t$, the values of d are noted and added to a set D . The stability bound is computed using equation (10). Appendix A describes the detailed numerical computation procedure.

At the distance d , the corresponding estimate of basin stability within one standard deviation error is reported in the confidence interval $[\hat{S}_B(X_D(d)) - e, \hat{S}_B(X_D(d)) + e]$. Due to the uncertainty in estimating the basin stability, the estimate of the stability bound can be reported in a confidence interval as well. The stability bound computed using the lower (upper) bound of the confidence interval of the estimated basin stability corresponds to the lower (upper) bound of the confidence interval of the estimated stability bound.

The maximum possible value of the lower bound of the confidence interval of the estimated basin stability is $1 - e$ (corresponding to an estimated basin stability of 1). If $1 - e < t$, then the lower bound of the confidence interval of the estimated stability bound is not defined. Thus, it is necessary that $t \leq 1 - e$ for the numerical estimation of stability bound to be tractable. Since $e \leq 0.5/\sqrt{n}$, the higher the value of t , the larger the number of sampled points required for stability bound computation. This probabilistic sampling procedure allows stability bound to be computable for any of basin of attraction. When $t = 1$, numerical errors are not tractable, and thus, the sampling procedure cannot be used to compute the stability bound.

III. RESULTS

A. Amazonian vegetation model

Using stability bound, we examine an ecological model of the Amazon rainforest^{8,10,20,21}. This model shows two stable states, one being a fertile forest state and the other being a barren savanna state. The model is described by the following differential equation:

$$\frac{dC}{dt} = \begin{cases} r(1-C)C - xC & \text{if } C > C_{\text{crit}} \\ -yC & \text{if } C < C_{\text{crit}} \end{cases} \quad (13)$$

C is the relative forest cover. C grows at a rate r and dies at a rate x , when C is greater than the critical forest cover C_{crit} . C dies at a rate y , when $C < C_{\text{crit}}$. The higher the aridity A of the region, the more the critical forest cover. We set $C_{\text{crit}} = A$.

This system has two fixed points, $C_F = 1 - x/r$ corresponding to the stable forest state, and $C_S = 0$ corresponding to the stable savanna state. The stable forest state exists if $C_F > C_{\text{crit}}$, and the stable savanna state exists if $C_{\text{crit}} > 0$. Factors such as global warming can affect the aridity of the rainforest, thus changing the critical forest cover. If the system is in the forest state, an increase in aridity can push the system past the bifurcation point, where the forest state ceases to exist. Linear stability fails to detect the change in stability of the forest state due to the shrinking of the basin of attraction captured in the state's basin stability⁸.

However, basin stability fails to capture the gradual loss in stability of the system near the bifurcation point. This is because basin stability is not related to the distance of the fixed point to the basin boundary. When the forest state is close to the bifurcation point, small perturbations in the direction of the basin boundary can push the system into the savanna state. Stability bound captures this aspect.

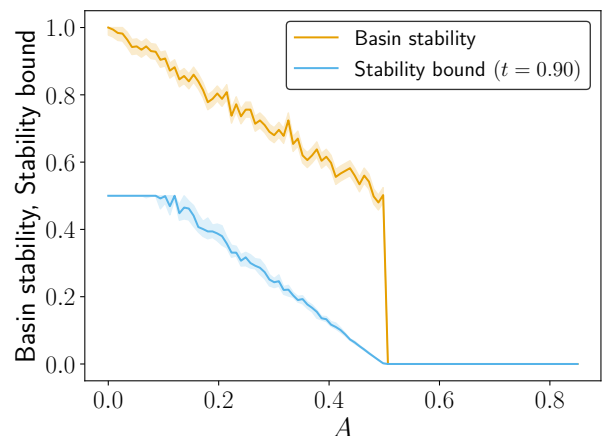


FIG. 1: Stability of the forest state. Basin stability and stability bound plotted versus aridity, A . The shaded region represents the error corresponding to \pm one standard deviation.

The parameters chosen for the differential equation are $r = 1$, $x = 0.5$ and $y = 1$. Basin stability and stability bound are computed in the phase space region $[0, 1]$. $n = 500$ sampled points are used for every basin stability computation.

Fig. 1 shows that the stability bound captures the gradual loss of stability near the bifurcation point of the forest state due to the decreasing distance of the boundary of the basin of attraction to the fixed point. Basin stability fails to capture this.

In Fig. 2, the stability bound is plotted for different values of the tolerance t . It shows that for all shown tolerance values, the gradual loss of stability of the forest state near the bifurcation point is captured.

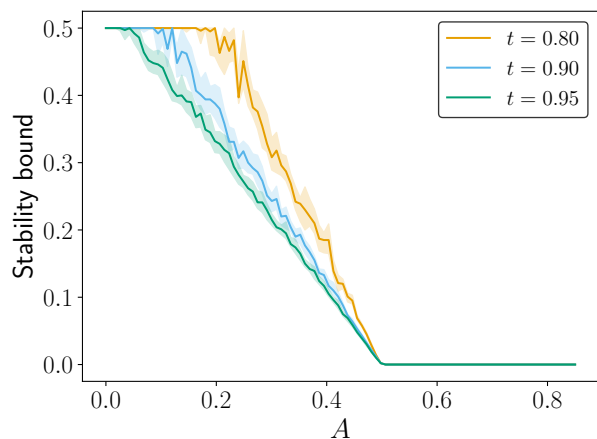


FIG. 2: Stability bound of the forest state versus Aridity A , for different values of the tolerance t . The shaded region represents the error of ± 1 standard deviation.

B. Ship capsize model

Waves and wind forces constantly buffet ships at sea, and under some conditions, ships may capsize. It is interesting to find the ship's stability against such perturbations.

The motion of a ship can be defined in six degrees of freedom²². We are concerned here with the motion of a ship in one specific degree of freedom: the rotation of a vessel about its longitudinal axis, which runs horizontally through the length of the ship. The ship's motion in this degree of freedom is called roll, which is responsible for capsizes.

The roll motion of a ship at sea can be modeled as²³

$$\ddot{x} + \beta\dot{x} + c(x) = F \sin(\omega t) \quad (14)$$

where x is the scaled roll angle of the ship, t is the scaled time, β is the damping coefficient of the ship, c is restoring moment of bouyancy forces. Forcing due to wind and waves in regular beam seas is assumed to be sinusoidal, with amplitude F and angular frequency ω .

In high winds, capsizing towards the wind is discounted. The restoring force in such conditions is modeled as $c(x) = x - x^2$. The restoring force $c(x)$ can be expressed in terms of a potential $v(x) = \frac{1}{2}x^2 - \frac{1}{3}x^3$, such that $c(x) = dv(x)/dx$. This potential has a local maxima at $x = 1$. Escape over the local maxima of this potential corresponds to capsize.

The equations describing the rolling motion of a ship in high winds can be written as

$$\dot{x} = y \quad (15a)$$

$$\dot{y} = -\beta\dot{x} - x + x^2 + F \sin(\omega t) \quad (15b)$$

These differential equations have been extensively studied before^{24–26}. The dynamical system described by the differential equations can have multiple attractors, all of which are desirable. The set of initial conditions that converge to the attractors of the system is known as the system's safe basin.

Thus, the safe basin describes the set of all states that are safe for the system and do not lead to capsizing.

With an increase in the forcing amplitude F , the safe basin gets eroded by fractal incursions, thus compromising the system's stability. This erosion of the safe basin of a system is known as basin erosion. To understand how basin erosion affects the stability of a system, various integrity measures that quantify the stability of such systems have been proposed^{17,27}. These integrity measures include the global integrity measure, which is the normalized volume of the safe basin, and the local integrity measure, which is the minimum distance from the attractor to the boundary of the safe basin in the Poincaré section. The global and local integrity measures are computed using a grid of points in the phase space. This numerical approach to compute the integrity measures is not robust, as the accuracy of the computed integrity measures is not quantifiable.

To have numerically robust stability measures, we define basin stability and stability bound analogous to the global integrity measure and local integrity measure, respectively, for the safe basin of the system. The basin stability of the safe basin is the fraction of states in a finite region X_P that are part of the safe basin \mathcal{B}' . It is given by

$$S_B(X_P) = \frac{\text{Vol}(X_P \cap \mathcal{B}')}{\text{Vol}(X_P)} \quad (16)$$

Stability bound, analogous to the local integrity measure, is defined from the attractor in the Poincaré section using the definition of basin stability in equation (16).

The parameters chosen for the differential equation are $\beta = 0.1$ and $\omega = 0.85$. An initial phase $\phi = \pi$ was chosen for the forcing term, such that the initial forcing is $-F$. The basin stability of the safe basin is computed in the region $X_P = [-0.8, 1.2] \times [-1, 1]$. The attractor corresponding to what would be observed physically under the slow increase of F from zero^{17,23} is considered. The stability bound is defined from this attractor in the Poincaré section at phase $\phi = \pi$. Stability bound is computed in the region $X_0 = \{z \in X | \text{dist}(z, z_0) < 1\}$, where X is the phase space, z_0 is the attractor in the Poincaré section at phase $\phi = \pi$, and $\text{dist}(z, z_0)$ is the Euclidean distance between $z = (x, y)$ and $z_0 = (x_0, y_0)$ defined as $\text{dist}(z, z_0) = \sqrt{a^2(x - x_0)^2 + b^2(y - y_0)^2}$. a and b are both taken to be unity with the dimensions of $1/x$ and $1/y$, respectively. $n = 500$ points are used for every basin stability computation.

In Figure 3, both basin stability and stability bound show a decrease in stability due to erosion of the safe basin on increasing the forcing amplitude F . Thompson et al.²³ observed that stability is compromised around $F \approx 0.07$. Around this value, the stability bound shows a sharp fall due to the attractor shifting close to the basin boundary. Basin stability does not capture this, thus highlighting the utility of stability bound as a measure of the system's integrity.

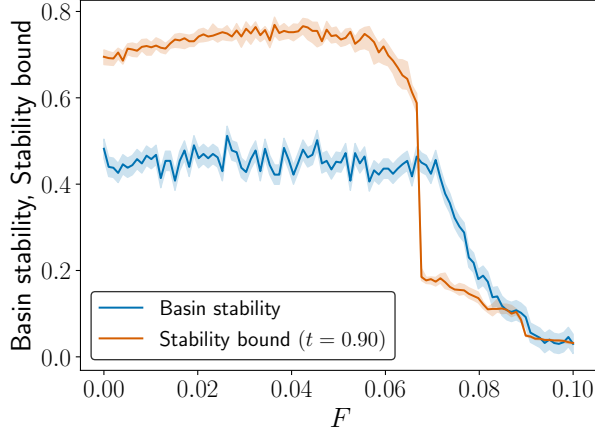


FIG. 3: Stability of a ship against capsizing. Basin stability and stability bound plotted versus the forcing amplitude, F . The shaded regions around the plots represent the error corresponding to the ± 1 standard deviation.

C. Power grids

Power grids facilitate the generation and consumption of electricity over vast geographical regions. During normal functioning, a power grid operates in its stable synchronous state, in which all parts of the grid function at the same frequency⁵. Power grids can be subject to many internal and external perturbations that can push the system out of its synchronous state. These perturbations can lead to a cascading failure, in which a small initial failure triggers a string of further failures^{28–30}. Such failures can propagate through the power grid and destabilize large parts of the grid. Cascading failures are devastating as they can result in large-scale power blackouts that can leave millions of people without electricity^{31–33}. Thus, it is vital to identify vulnerabilities in power grids in order to prevent future grid failures.

We use a complex network power grid representation to model power grids with nodes as generators and consumers and edges as transmission lines. Generators and consumers are modeled using the swing equation⁵. The equations that describe the dynamics of the grid are^{15,34}

$$\dot{\theta}_i = \omega_i \quad (17a)$$

$$\dot{\omega}_i = -\alpha_i \omega_i + P_i - \sum_{j=1}^N K_{ij} \sin(\theta_i - \theta_j), \quad (17b)$$

where, for the i^{th} node,

θ_i is the phase angle in the frame rotating at the synchronous grid frequency,

ω_i is the angular velocity in the frame rotating at the synchronous grid frequency,

α_i is the damping factor,

P_i is the net power generated or consumed.

K_{ij} is the transmission capacity between node i and node j , provided they are connected to each other. If node i and node j are not connected, then $K_{ij} = 0$.

The fixed point of equation (17) corresponds to the stable synchronous state of the grid. In this state, the i^{th} node has the phase θ_i^s and frequency 0. There also exist several undesirable non-synchronous states in which perturbations can push the grid to^{15,34,35}. To study the effect of finite perturbations on individual nodes in a grid, a variant of basin stability known as single-node basin stability has been introduced¹⁵. The single-node basin stability of node i in the network is the basin stability corresponding to perturbations only hitting the node i (perturbations to θ_i and ω_i) from the initial synchronous state. If single-node perturbations occur in the region X_{sn} , such that $(\theta_i, \omega_i) \in X_{sn}$ is a single-node perturbation at the i^{th} node, then, the single-node basin stability of node i is the basin stability with perturbations conditioned in the region

$$X_i^0 = \{(\theta, \omega) \in X \mid (\theta_i, \omega_i) \in X_{sn} \wedge (\forall j \neq i : \theta_j = \theta_j^s \wedge \omega_j = 0)\} \quad (18)$$

where $\theta = (\theta_1, \theta_2, \dots, \theta_N)$ and $\omega = (\omega_1, \omega_2, \dots, \omega_N)$.

Complementary to single-node basin stability, we define a variant of stability bound called single-node stability bound. The single-node stability bound of node i is the stability bound with perturbations conditioned to the node i from the initial synchronous state. The region of perturbations for the single-node stability bound of node i is given by X_i^0 if single-node perturbations occur in the region X_{sn} .

To identify how network structure affects single-node stability, we compute each node's single-node basin stability and the single-node stability bound of several synthetic power grid networks. 200 Erdős–Rényi networks, each with 40 nodes and 54 edges, were generated for this. In each network, half of the nodes were taken to be generators, and half of the nodes were taken to be consumers. The following parameters were used: $K = 8$ for every transmission line, $\alpha = 0.1$ for every node, $P = 1$ for every generator, and $P = -1$ for every consumer. We choose $X_{sn} = [-\pi, \pi] \times [-100, 100]$. The single-node basin stability of node i is computed in the region X_i^0 given by equation (18). The single-node stability bound of node i is computed in the region $\{x \in X_i^0 \mid \text{dist}(x, \mathcal{A}) \leq 15\}$, where \mathcal{A} is the synchronous state of the grid. The distance between a state in the phase space to the attractor is $\text{dist}(x, \mathcal{A}) = \sqrt{\sum_{i=0}^N [a^2(\theta_i - \theta_i^s)^2 + b^2\omega_i^2]}$. a and b are both taken to be unity with the dimensions of $1/\theta_i$ and $1/\omega_i$, respectively. The stability bound is computed with a tolerance $t = 0.9$, and $n = 500$ points are used for every basin stability computation.

The total number of nodes in all the networks amounts to $40 \times 200 = 8,000$. Fig. 4 shows the distribution of the single-node basin stability and the single-node stability bound of all these 8,000 nodes. Nodes present in the lower end of these distributions are vulnerable. We seek to study the local topological properties of these nodes. Previous studies have shown how network topology affects power grid stability^{15,36–38}. It has been found that based on single-node basin stability, nodes inside dead ends and dead trees are likely to be less stable¹⁵. The stability of such network motifs can be better understood by studying the relation between single-node stability and a network centrality measure known as betweenness centrality.

Betweenness centrality measures the importance of a node in a network based on how many shortest paths pass through it. The betweenness centrality of node i in a network is defined as³⁹

$$b_i = \sum_{j \neq i, k \neq i, k > j} \frac{\sigma_{jk}^i}{\sigma_{jk}} \quad (19)$$

where σ_{jk}^i is the number of shortest paths from node j to node k which pass through node i , and σ_{jk} is the number of shortest paths which pass from node j to node k .

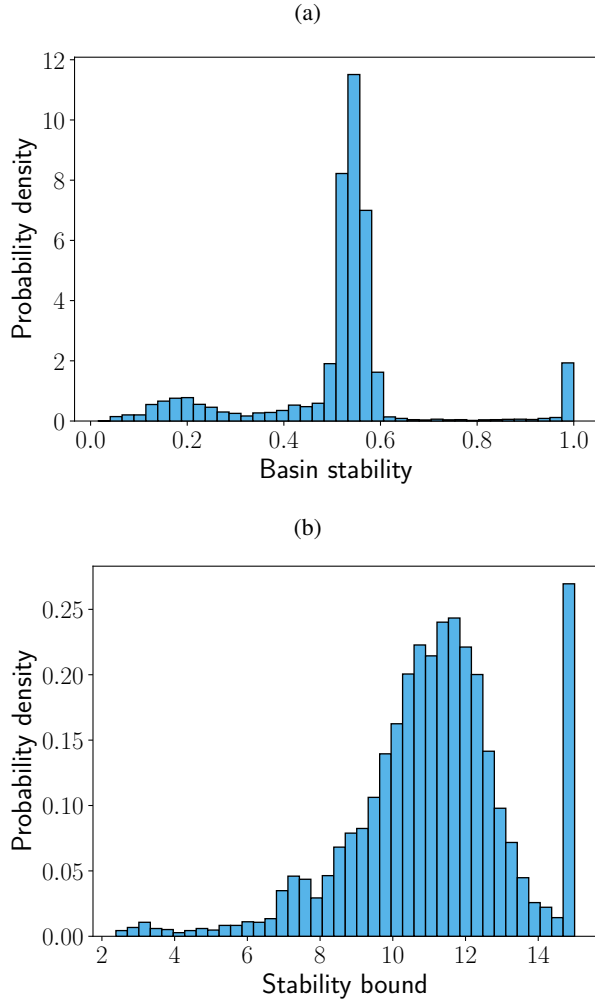


FIG. 4: Distribution of the (a) single-node basin stability and the (b) single-node stability bound for all nodes in all the generated networks.

In Fig. 5a, marked dips in the single-node basin stability are observed corresponding to betweenness centrality values of $N - 2$, $2N - 6$, and $2N - 5$, where N is the number of nodes in the networks (here, $N = 40$). These dips correspond to nodes inside dead ends and dead trees¹⁵. In Fig. 5b, dips in the single-node stability bound are observed at the same betweenness centrality values as the dips of single-node basin stability in Fig. 5a. In addition to these dips, a marked dip in

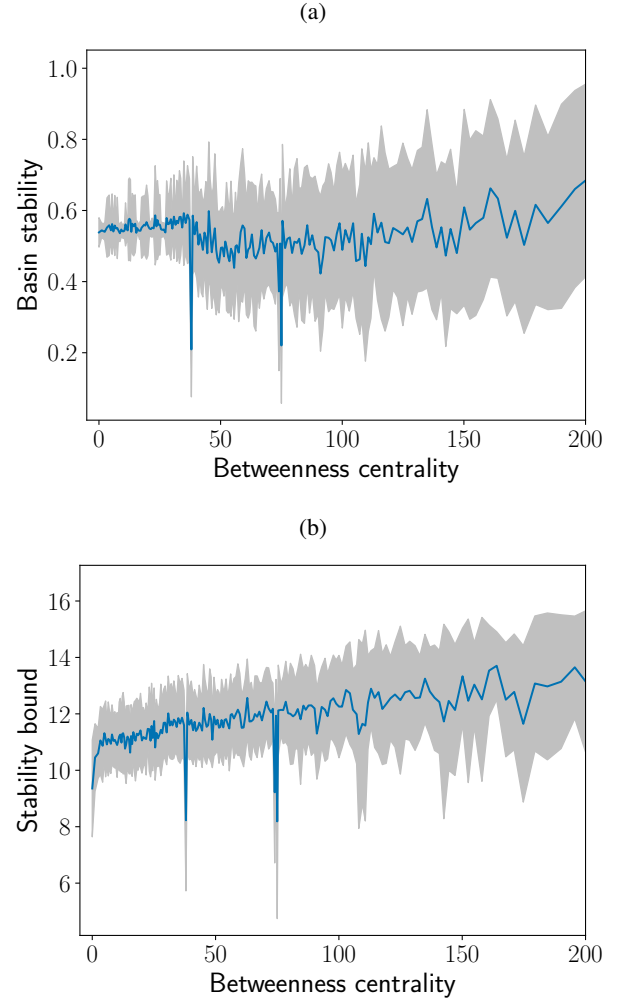


FIG. 5: The dependence of single-node stability on betweenness centrality. (a) Single-node basin stability versus betweenness centrality. (b) Single-node stability bound versus betweenness centrality. The blue line shows the average trend, and the grey region indicates the error corresponding to ± 1 standard deviation

the single-node stability bound corresponding to a betweenness centrality of 0 is observed. This dip corresponds to dead-end nodes of networks, consisting of over twenty percent of nodes in all the generated networks. Like single-node basin stability, single-node stability bound characterizes nodes inside dead ends and dead trees as less stable. However, unlike single-node basin stability, single-node stability bound characterizes dead ends as less stable.

IV. CONCLUSION

We have introduced a novel stability quantifier for dynamical systems that overcomes some of the limitations of basin stability and stability threshold and have successfully shown its applicability to real-world systems.

In many engineering and socio-ecological systems, the minimum distance from an attractor to its basin boundary aids in quantifying the system’s resilience^{16,17}. This distance can be computed using the stability threshold approach¹² as long as the basin boundaries are smooth. However, for systems with non-smooth basin boundaries, the stability threshold approach becomes inadequate. The applicability of stability bound to non-smooth basin boundaries opens up a host of systems on which distance-based resilience can be quantified.

In the case of the Amazon rainforest model, we have observed how stability bound provides early warning signs before the loss of stability of the forest state. These early warning signs are not observed in the basin stability of the forest state. In the ship capsizing model, the stability bound provides a much better indicator of an impending catastrophe.

In power grids, due to the fractal nature of basin of attraction slices⁴⁰, stability threshold cannot be employed as a measure of single-node stability. We have successfully introduced stability bound as a distance-based stability quantifier to quantify the single-node stability of power grids. We have found that the single-node stability bound identifies vulnerabilities in a large class of nodes that have not been previously detected as vulnerable according to single-node basin stability. To complement basin stability, we believe that stability bound can be employed to examine power grid stability.

V. ACKNOWLEDGEMENTS

We are thankful to Arnab Acharya for the valuable discussions. S. Banerjee acknowledges the J C Bose National Fellowship provided by SERB, Government of India, Grant No. JBR/2020/000049.

VI. AUTHOR DECLARATIONS

A. Conflict of interest

The authors have no conflicts to disclose.

B. Author contributions

Calvin Alvares proposed the new measure, the ‘stability bound’, simulated the example systems and demonstrated its utility.

Soumitro Banerjee was responsible for conceptualizing the problem, developing the idea, and checking the validity of the results.

VII. DATA AVAILABILITY

Data sharing is not applicable to this article as no new data were created or analyzed in this study.

Appendix A

The procedure to compute the stability bound is described below. A finite region of the phase space, X_0 , is considered. The basin stability $\hat{S}_B(X_D(d))$ is computed using n sampled points from $d = d_{\max}$ to $d = d_0$ with a finite step size δ . $X_D(d)$ is defined in equation (5), d_{\max} is defined in equation (9), and d_0 is the largest distance such that $\hat{S}_B(X_D(d_0)) = 1$. For the basin stability computation $\hat{S}_B(X_D(d - \delta))$, sampled points from the previous basin stability computation $\hat{S}_B(X_D(d))$ that fall in the region $X_D(d - \delta)$, are reused. This significantly reduces the total number of sampled points required for the computation of stability bound.

Between two consecutive distances $d + \delta$ and d , the basin stability $S_B(X_D(d'))$ for $d' \in (d, d + \delta)$ is not known. If the basin stability $S_B(X_D(d))$ is known, then for $d' \in [d, d + \delta]$, $S_B(X_D(d')) \geq S_B(X_D(d)) (d/(d + \delta))^N$. The worst case estimate of basin stability for $d' \in [d, d + \delta]$ is $\hat{S}_B^t(X_D(d), X_D(d + \delta)) = \hat{S}_B(X_D(d)) (d/(d + \delta))^N$.

If the estimated basin stability $\hat{S}_B(X_D(d_{\max})) < t$, the value d_{\max} is added a set D . For $d = \{d_0, d_0 + \delta, \dots, d_{\max} - \delta\}$, if the worst case basin stability estimate $\hat{S}_B^t(X_D(d), X_D(d + \delta)) < t$, the values of d are noted and added to a set D . The stability bound is then calculated using equation (10).

¹U. Feudel, A. N. Pisarchik, and K. Showalter, “Multistability and tipping: From mathematics and physics to climate and brain—minireview and preface to the focus issue,” *Chaos: An Interdisciplinary Journal of Nonlinear Science* **28** (2018).

²W. W. Lytton, “Computer modelling of epilepsy,” *Nature Reviews Neuroscience* **9**, 626–637 (2008).

³R. M. May, “Thresholds and breakpoints in ecosystems with a multiplicity of stable states,” *Nature* **269**, 471–477 (1977).

⁴A. Robinson, R. Calov, and A. Ganopolski, “Multistability and critical thresholds of the Greenland ice sheet,” *Nature Climate Change* **2**, 429–432 (2012).

⁵J. Machowski, Z. Lubosny, J. W. Bialek, and J. R. Bumby, *Power system dynamics: stability and control* (John Wiley & Sons, 2020).

⁶L. M. Pecora and T. L. Carroll, “Master stability functions for synchronized coupled systems,” *Physical review letters* **80**, 2109 (1998).

⁷S. H. Strogatz, *Nonlinear dynamics and chaos with student solutions manual: With applications to physics, biology, chemistry, and engineering* (CRC press, 2018).

⁸P. J. Menck, J. Heitzig, N. Marwan, and J. Kurths, “How basin stability complements the linear-stability paradigm,” *Nature physics* **9**, 89–92 (2013).

⁹F. Hellmann, P. Schultz, C. Grabow, J. Heitzig, and J. Kurths, “Survivability of deterministic dynamical systems,” *Scientific reports* **6**, 29654 (2016).

¹⁰C. Mitra, J. Kurths, and R. V. Donner, “An integrative quantifier of multistability in complex systems based on ecological resilience,” *Scientific reports* **5**, 16196 (2015).

¹¹C. Mitra, A. Choudhary, S. Sinha, J. Kurths, and R. V. Donner, “Multiple-node basin stability in complex dynamical networks,” *Physical Review E* **95**, 032317 (2017).

¹²V. V. Klinshov, V. I. Nekorkin, and J. Kurths, “Stability threshold approach for complex dynamical systems,” *New Journal of Physics* **18**, 013004 (2015).

¹³L. Halekotte and U. Feudel, “Minimal fatal shocks in multistable complex networks,” *Scientific reports* **10**, 11783 (2020).

¹⁴V. V. Klinshov, S. Kirillov, J. Kurths, and V. I. Nekorkin, “Interval stability for complex systems,” *New Journal of Physics* **20**, 043040 (2018).

¹⁵P. J. Menck, J. Heitzig, J. Kurths, and H. Joachim Schellnhuber, “How dead ends undermine power grid stability,” *Nature communications* **5**, 3969 (2014).

- ¹⁶B. Walker, C. S. Holling, S. R. Carpenter, and A. Kinzig, “Resilience, adaptability and transformability in social–ecological systems,” *Ecology and society* **9** (2004).
- ¹⁷M. S. Soliman and J. M. T. Thompson, “Integrity measures quantifying the erosion of smooth and fractal basins of attraction,” *Journal of Sound and Vibration* **135**, 453–475 (1989).
- ¹⁸J. Aguirre, R. L. Viana, and M. A. Sanjuán, “Fractal structures in nonlinear dynamics,” *Reviews of Modern Physics* **81**, 333 (2009).
- ¹⁹R. Delabays, M. Tyloo, and P. Jacquod, “The size of the sync basin revisited,” *Chaos: An Interdisciplinary Journal of Nonlinear Science* **27** (2017).
- ²⁰L. Da Silveira Lobo Sternberg, “Savanna–forest hysteresis in the tropics,” *Global Ecology and Biogeography* **10**, 369–378 (2001).
- ²¹M. Hirota, M. Holmgren, E. H. Van Nes, and M. Scheffer, “Global resilience of tropical forest and savanna to critical transitions,” *Science* **334**, 232–235 (2011).
- ²²K. J. Rawson and E. C. Tupper, *Basic Ship Theory Volume 1*, Vol. 1 (Butterworth-Heinemann, 2001).
- ²³J. M. T. Thompson, R. C. T. Rainey, and M. S. Soliman, “Ship stability criteria based on chaotic transients from incursive fractals,” *Philosophical Transactions of the Royal Society of London. Series A: Physical and Engineering Sciences* **332**, 149–167 (1990).
- ²⁴J. M. T. Thompson, S. R. Bishop, and L. M. Leung, “Fractal basins and chaotic bifurcations prior to escape from a potential well,” *Physics Letters A* **121**, 116–120 (1987).
- ²⁵J. M. T. Thompson, “Chaotic phenomena triggering the escape from a potential well,” *Proceedings of the Royal Society of London. A. Mathematical and Physical Sciences* **421**, 195–225 (1989).
- ²⁶J. M. T. Thompson and Y. Ueda, “Basin boundary metamorphoses in the canonical escape equation,” *Dynamics and stability of systems* **4**, 285–294 (1989).
- ²⁷J. M. T. Thompson, “Dynamical integrity: three decades of progress from macro to nanomechanics,” *Global nonlinear dynamics for engineering design and system safety*, 1–26 (2019).
- ²⁸S. V. Buldyrev, R. Parshani, G. Paul, H. E. Stanley, and S. Havlin, “Catastrophic cascade of failures in interdependent networks,” *Nature* **464**, 1025–1028 (2010).
- ²⁹A. E. Motter and Y.-C. Lai, “Cascade-based attacks on complex networks,” *Physical Review E* **66**, 065102 (2002).
- ³⁰B. Schäfer, D. Witthaut, M. Timme, and V. Latora, “Dynamically induced cascading failures in power grids,” *Nature communications* **9**, 1975 (2018).
- ³¹C. E. R. C. (CERC), “Report on the grid disturbances on 30th July and 31st July 2012,” Tech. Rep. (2012).
- ³²Project Group Turkey, “Report on blackout in Turkey on 31st March 2015,” Tech. Rep. (European Network of Transmission System Operators for Electricity (ENTSO-E), 2015).
- ³³Union for the Coordination of Transmission of Electricity (UCTE), “Final report of the investigation committee on the 28th September 2003 blackout in Italy,” Tech. Rep. (European Network of Transmission System Operators for Electricity (ENTSO-E), 2003).
- ³⁴G. Filatrella, A. H. Nielsen, and N. F. Pedersen, “Analysis of a power grid using a Kuramoto-like model,” *The European Physical Journal B* **61**, 485–491 (2008).
- ³⁵H.-D. Chiang, *Direct methods for stability analysis of electric power systems: theoretical foundation, BCU methodologies, and applications* (John Wiley & Sons, 2011).
- ³⁶H. Kim, S. H. Lee, and P. Holme, “Building blocks of the basin stability of power grids,” *Physical Review E* **93**, 062318 (2016).
- ³⁷J. Nitzbon, P. Schultz, J. Heitzig, J. Kurths, and F. Hellmann, “Deciphering the imprint of topology on nonlinear dynamical network stability,” *New Journal of Physics* **19**, 033029 (2017).
- ³⁸P. Schultz, J. Heitzig, and J. Kurths, “Detours around basin stability in power networks,” *New Journal of Physics* **16**, 125001 (2014).
- ³⁹L. C. Freeman, “A set of measures of centrality based on betweenness,” *Sociometry*, 35–41 (1977).
- ⁴⁰L. Halekotte, A. Vanselow, and U. Feudel, “Transient chaos enforces uncertainty in the British power grid,” *Journal of Physics: Complexity* **2**, 035015 (2021).